Acta Pharmaceutica Sinica B 2020;10(4):667−679

Chinese Pharmaceutical Association
Institute of Materia Medica, Chinese Academy of Medical Sciences

Acta Pharmaceutica Sinica B

www.elsevier.com/locate/apsb
www.sciencedirect.com

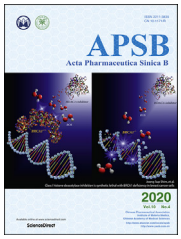

ORIGINAL ARTICLE

Combinatory antitumor therapy by cascade targeting of a single drug

Aiyun Liu[a,†], Huaisong Wang[a,†], Xiaoshuang Hou[a], Yu Ma[a], Gongjun Yang[a], Yanglong Hou[b,*], Ya Ding[a,*]

[a]*Key Laboratory of Drug Quality Control and Pharmacovigilance, Ministry of Education, China Pharmaceutical University, Nanjing 210009, China*
[b]*Beijing Key Laboratory for Magnetoeletric Materials and Devices, Beijing Innovation Center for Engineering Science and Advanced Technology, Department of Materials Science and Engineering, College of Engineering, Peking University, Beijing 100871, China*

Received 19 June 2019; received in revised form 19 July 2019; accepted 11 August 2019

KEY WORDS

Combin chemotherapy;
Single drug;
Paclitaxel;
Microtubules;
Mitochondria;
Cytotoxicity

Abstract Combination therapy has shown its promise in the clinic for enhancing the efficacy of tumor treatment. However, the dose control of multiple drugs and their non-overlapping toxicity from different drugs are still great challenge. In this work, a single model drug, paclitaxel (PTX), is used to realize combination therapy and solve the problems mentioned above. Either PTX or its triphenylphosphine derivative (TPTX) is encapsulated in galactose-modified liposomes (GLips) to obtain GLips-P or GLips-TP, which are simply mixed in different ratios to finely control the proportion of PTX and TPTX. These mixed liposomes, GLips-P/TP, feature a cascade target delivery of PTX, from tissue to cell, and then to organelle. PTX plays a primary role to cause the cytotoxicity by microtubule bindings in cytoplasm, while TPTX is proved to increase the intracellular levels of caspase-3 and caspase-9 that cause apoptosis *via* a mitochondria-mediated pathway. Notably, GLips-P/TP 3:1 exhibited the significant drug synergy in both cytotoxicity assay of HepG2 cells and the treatment efficacy in Heps xenograft ICR mouse models. This work not only demonstrates the great promise of a cascade targeting delivery for precise tumor treatment, but also offers a novel platform to design combinatory therapy systems using a single drug.

*Corresponding authors. Tel./fax: +86 25 83271326.
E-mail addresses: hou@pku.edu.cn (Yanglong Hou), dingya@cpu.edu.cn (Ya Ding).
[†]These authors made equal contributions to this work.
Peer review under the responsibility of Chinese Pharmaceutical Association and Institute of Materia Medica, Chinese Academy of Medical Sciences.

https://doi.org/10.1016/j.apsb.2019.08.011

1. Introduction

Combination chemotherapy has been widely explored and shown its promise in the clinic for enhancing the efficacy of cancer treatment[1−4]. Multiple drugs that each utilizes unique molecular mechanism have been combined to achieve drug synergy[3], decrease therapeutic doses, reduce the chance of multidrug resistance, and minimize overlapping toxicity[5]. However, the current administration of combination regimens suffers from varying pharmacokinetics among different drugs, which lead to a complicated dosing regimen and poor patient compliance. With the emergence of nanotechnology, encapsulating various drugs simultaneously in a nanocarrier offers an unparalleled opportunity to unify the pharmacokinetics of each drug, which has been fully reviewed in recent literatures[2,5]. However, the issues of the dose control of different drugs, the unpredictable interactions between multiple drugs, and their possibly non-overlapping toxicity in this combinatory system are still great challenge.

Alternatively, if effective multi-target treatments can be achieved using a single drug, the controllability and effectiveness of the combination therapy, as well as its safety, will be greatly enhanced. In fact, many anticancer drugs show their activities *via* multiple signal pathways, such as paclitaxel (PTX)[6], doxorubicin (DOX)[7], curcumin[8], and α-tocopherol[9]. In addition to their primary treatment mechanisms, mitochondria-related signal pathway is commonly involved in their therapeutic processes. For example, PTX is largely believed to exert its action by stabilizing the microtubules of tumor cells[10,11], and it has been also reported to act directly on isolated mitochondria from human neuroblastoma cells to induce the permeability transition pore-dependent release of cytochrome C[12]. Moreover, when DOX binds to DNA-associated enzymes and intercalates with DNA base pairs[13,14], it also generates reactive oxygen and nitrogen species in mitochondria[15,16]. This means that these chemotherapy agents could aim to multiple targets, resulting in a range of cytotoxic effects *via* both the biomacromolecule damage and mitochondrial injury mechanisms. In these cases, the function inhibition of biological macromolecules plays a major role in the antitumor mechanism, while the environment regulation of mitochondria is an auxiliary mechanism. Therefore, either PTX or DOX has been loaded in mitochondria-targeted carriers to play their antitumor activities[17−19]. However, the therapy combining the major and auxiliary therapeutic mechanisms of one chemical drug is usually ignored, even though it would achieve a more controllable structure, clearer mechanism of action, and improved efficacy and biosafety.

In this work, to confirm our hypothesis, a mitochondria-target ligand (triphenylphosphine, TPP) was attached on PTX to enhance its effect through the mitochondria-mediated mechanism. Either PTX or its triphenylphosphine derivative (TPTX) is encapsulated in the galactose-modified liposomes (GLips) to obtain GLips-P or GLips-TP, respectively, which are simply mixed in different ratios to finely control the proportion of PTX and TPTX in mixed liposomes (GLips-P/TP, Fig. 1). Utilizing the designed liposomes, PTX experienced a cascade targeting process, *e.g.*, the liver tumor, tumor cells, and then mitochondria in succession. It was worth noting that, when 25% PTX was replaced by TPTX in mixed liposomes, *e.g.*, GLips-P/TP 3:1, the contribution of auxiliary therapeutic mechanism related to mitochondria was obviously enhanced and showed the best drug synergy even though only one drug was used. Therefore, this work provides a brand-new perspective for liver cancer treatment, *e.g.*, the realization of combinatory therapy using a cascade target delivery of one single drug.

2. Materials and methods

2.1. Materials

PTX was acquired from Yew Pharmaceutical Co. (Jiangsu, China). 1,2-Distearoyl-*sn*-glycero-3-phosphoethanolamine-*N*-[methoxy (polyethyleneglycol)-2000] (DSPE-PEG, MW 2000 Da, 93%) and 1,2-distearoyl-*sn*-glycero-3-phosphoethanolamine-*N*-[amino (polyethyleneglycol)-2000] (DSPE-PEG-NH_2, MW 2000 Da, 93%) were purchased from A. V. T. Pharmaceutical Co., Ltd. (Shanghai, China). Fluorescein (FR, 95%) was obtained from Bide Pharmatech Ltd. (Shanghai, China). Lactobionic acid (LA, 97%), 5-aminofluorescein (5-AFR, 96%), (4-carboxybutyl) triphenylphosphonium bromide (TPP-COOH, 98%), and 1-ethyl-3-(3-dimethyllaminopropyl) carbodiimide hydrochloride (EDC·HCl, 98%) were purchased from Aladdin Biochemical Technology Co., Ltd. (Shanghai, China). *N*-Hydroxysuccinimide (NHS, 98%) was provided by Jingchun Reagent Co., Ltd. (Shanghai, China). Soya phosphatidyl choline (SPC, S100) and cholesterol were supplied by GmbH Lipoid (Ludwigshafen, Germany) and Shanghai Huixing Biochemical Reagent Co., Ltd. (China). Unless otherwise stated, all starting materials were obtained from commercial suppliers and used without further purification. Solvents were dried using standard procedures. All aqueous solutions were prepared using deionized water (>18 ΩU, Purelab Classic Corp., Harrogate, UK).

2.2. Instrumental methods

Fourier Transform Infrared Spectroscopy (FT-IR) spectra were collected on a Nicolet 6700 FT-IR spectrometer (Thermo Scientific, Harrogate, UK). The Proton Nuclear Magnetic Resonance Spectroscopy (^{1}H NMR) spectra were recorded on a Bruker (AVANCE) AV-300 spectrometer (MA, USA). Ultraviolet−visible (UV−Vis) spectra were recorded on a UV-2401 PC UV−Vis spectrophotometer (Shimadzu, Kyoto, Japan). Transmission electron microscope (TEM) images were performed using a JEM-2100 TEM instrument with an acceleration voltage of 200 kV (JEOL JEM, Japan). The fluorescence emission spectra were measured using an RF-5301 PC spectrofluorophotometer (Shimadzu, Kyoto, Japan). The hydrodynamic diameters and zeta potentials were obtained using a zeta potential analyzer (ZetaPlus, Brukehaven Instruments Coorporation, New York, USA). Analytical reverse-phase high performance liquid chromatography (RP-HPLC) was performed using a Shimadzu-20AT series with a Thermo BDS HYPERSIL C18 reversed-phase chromatography column (150 mm × 4.6 mm, 5 μm) and a UV detector set at 227 nm. All HPLC runs were performed in triplicate.

2.3. The synthesis of DSPE-PEG-LA

To offer an active liver targeting function in liposomes, DSPE-PEG-LA was synthesized by acylation reaction of DSPE-PEG-NH_2 and LA under the catalysis of EDC·HCl and NHS. White powders of DSPE-PEG-NH_2 (50 mg, 0.018 mmol) and LA (64.5 mg, 0.18 mmol) were dissolved in 2 mL DMSO, respectively, and stirred at room temperature for 2 h. And then,

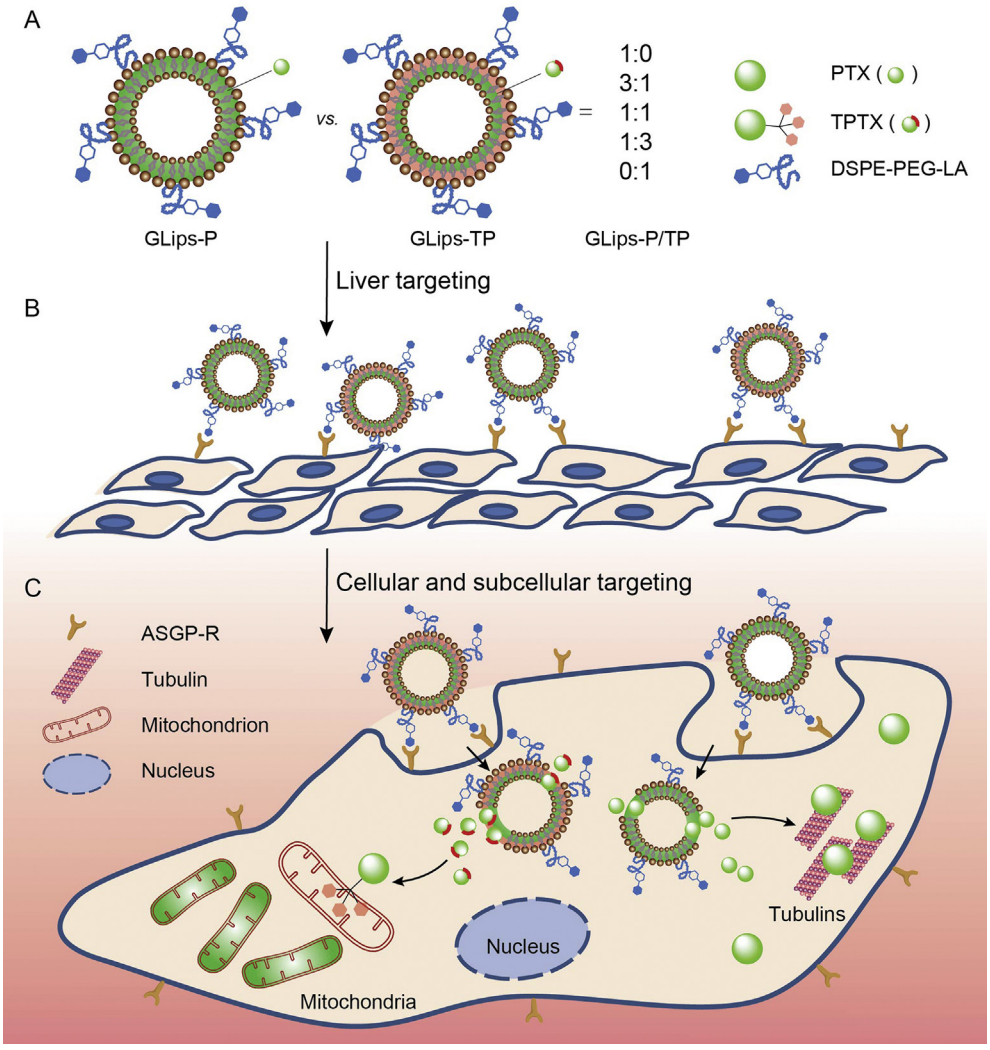

Figure 1 Schematic illustration of mixed liposomes for combination therapy *via* cascade target delivery of a chemical drug. (A) The preparation and structure of cascade targeting liposomes. (B) The liver targeting of liposomes based on the surface modification of galactose moiety and their asialoglycoprotein receptor (ASGP-R)-mediated recognition. (C) The internalization of liposomes *via* the receptor-mediated endocytosis and the subsequent tubulin and mitochondrion targeting of drugs for the tumor cell inhibition.

EDC·HCl (34.5 mg, 0.18 mmol), NHS (20.7 mg, 0.18 mmol), and triethylamine (TEA, 3 μL) were added into the mixture to stirred overnight at room temperature. The reaction solution was dialyzed (MWCO 2000 Da) against deionized water for 24 h. The product was lyophilized to obtain white powder (47.5 mg, yield 84.7%). ^{1}H NMR (DMSO-d_6): δ 0.85 (s, 6H), 1.23 (s, 64H), 3.31−3.51 (m, 180H, broad), 3.74 (s, 4H), 3.86 (s, 2H), 4.72 (s, 1H), 7.90 (s, 2H). IR (KBr): υ_{max} 3407, 2917, 2888, 1740, 1660, 1547, 1334, 1111, 721 cm^{-1}.

2.4. *The synthesis of TPP-modified FR (TFR)*

TPP-COOH (57 mg, 0.13 mmol), EDC·HCl (33 mg, 0.18 mmol), and 1-hydroxybenzotriazole (HOBt, 24 mg, 0.18 mmol) were dissolved in 3 mL of *N*,*N*-dimethylformamide (DMF) and stirred for 20 h. Under rigorous agitation, 5-AFR (30 mg, 0.09 mmol) and 4-dimethylaminopyridine (DMAP) (15 mg, 0.12 mmol) in 3 mL of DMF were slowly added into the reaction mixture drop by drop. The mixture was stirred for 24 h under room temperature. 10 mL deionized water was added to the mixture and then orange solid was separated out. Filter and wash the sediment with deionized water and dichloromethane (DCM) for three times. The crude product was purified by column chromatography and eluted with dichloromethane:methanol = 8:1 (R_f = 0.30). The final product (45 mg, 64.5%) was obtained as orange powder. ^{1}H NMR (DMSO-d_6): δ 1.67 (s, 2H), 1.95 (s, 2H), 2.65 (s, 2H), 3.75 (s, 2H), 5.75 (s, 1H), 6.34 (s, 2H), 6.55 (d, 2H), 6.66 (d, 1H), 6.81 (d, 1H), 6.92 (s, 1H), 7.15 (s, 1H), 7.77 (d, 15H), 7.82 (s, 2H), 7.91 (s, 1H), 10.05 (s, 2H). FT-IR (KBr): υ_{max} 3343, 2919, 1745, 1660, 1604, 1587, 1503, 1460, 1438, 1382, 1320, 1107, 908, 847, 583 cm^{-1}.

2.5. *Synthesis of TPTX*

Firstly, the synthesis of 2′-TBS-PTX was referred to our previous report[20]. 2′-TBS-PTX (300 mg, 0.31 mmol), TPP-COOH (824 mg, 1.86 mmol) and DMAP (113 mg, 0.93 mmol) were dissolved in 10 mL of DCM. Under vigorous stirring for 10 min, *N*,*N*′-diisopropylcarbodiimide (DIC, 547 mg, 4.34 mmol) in 5 mL of DCM was added dropwise to the reaction mixture. After being stirred for 24 h, the reaction mixture was diluted by DCM and

washed with water. The organic extract was concentrated under reduced pressure, and the crude product was further purified by column chromatography with dichloromethane:methanol = 40:1 (R_f = 0.40, Yield 46.3%) to obtain 2′-TBS-7-TPP-PTX. ^{1}H NMR (300 MHz, $CDCl_3$): δ 0.03 (s, 3H), 0.08 (s, 3H), 0.81 (s, 9H), 1.02 (s, 3H), 1.08 (m, 3H), 1.24 (s, 3H), 1.69 (broad, 4H), 2.01 (s, 2H), 2.46 (broad, 4H), 2.50 (s, 3 H), 3.58 (m, 3H), 3.73 (d, 1H), 4.07 (s, 2H), 4.80 (d, 2H), 5.00 (d, 1H), 5.41 (m, 1H), 5.54 (t, 1H), 5.99 (s, 1H), 7.38 (t, 1H), 7.40 (t, 1H), 7.52 (m, 5H), 7.76 (m, 2H), 7.80 (m, 16H), 7.81 (m, 1H), 7.86 (m, 6H), 8.00 (d, 2H), 8.76 (d, 1H). FT-IR (KBr): υ_{max}: 3415, 2950, 2847, 1734, 1667, 1618, 1530, 1486, 1245, 1180, 1064, 984, 845, 772, 707 cm^{-1}.

2′-TBS-7-TPP-PTX (160 mg, 0.11 mmol) was dissolved in 2 mL of tetrahydrofuran (THF). Under vigorous stirring for 10 min, tetrabutylammonium fluoride (TBAF, 10 drops, 1 mol/L in THF) in 3 mL of THF was added dropwise to the reaction mixture. After being stirred for 6 h, THF was removed under reduced pressure and the reaction mixture was diluted by DCM and washed with water. The organic extract was concentrated under reduced pressure, and the crude product was further purified by column chromatography with dichloromethane:methanol = 50:1 (R_f = 0.40, Yield 61.31%) to obtain TPTX. ^{1}H NMR (300 MHz, DMSO-d_6): δ 1.04 (s, 4H), 1.17 (m, 4H), 1.23 (s, 2H), 1.41 (s, 3H), 1.55 (s, 4H), 1.63 (m, 4H), 1.74 (s, 3H), 2.16 (s, 3H), 2.24 (s, 2H), 2.35 (m, 3H), 3.70 (m, 1H), 4.05 (s, 2H), 4.052 (s, 2H), 4.61 (t, 1H), 4.78 (s, 1H), 4.92 (d, 1H), 5.42 (t, 1H), 5.92 (s, 2H), 6.032 (s, 1H), 6.04 (s, 1H), 6.14 (d, 1H), 7.39 (t, 1H), 7.47 (t, 4H), 7.52 (m, 9H), 7.54 (m, 2H), 7.63 (m, 6H), 7.89 (d, 2H), 7.97 (d, 2H), 8.86 (d, 1H). FT-IR (KBr): υ_{max} 2944, 2888, 1736, 1660, 1603, 696 cm^{-1}.

2.6. *Preparation of liposomes*

Liposomes were prepared based on the thin-film dispersion method[21,22]. Lipids of SPC (98.3 mg), cholesterol (20.0 mg), and DSPE-PEG (6.75−27.00 mg)/DSPE-PEG-LA (7.50−30.00 mg) (the molecular concentration of DSPE-PEG-LA in the liposomes was 0.67%, 1.34% or 2.68%) were dissolved in 9 mL chloroform in a round-bottomed flask. Either FR (0.5 mg) or TFR (1.2 mg) was respectively dissolved in 1 mL methanol and well mixed with the chloroform solutions described above. The organic solvent was evaporated and dried under vacuum rotary for 30 min to form a dried thin lipid film. This film was then hydrated in 10 mL deionized water with vigorous vortexing for 30 min, and then applied with ultrasound for 30 min at 15% power (total 650 W) in an ice-water bath. The as prepared FR- and TFR-encapsulated liposomes with and without galactose modification including Lips-F, Lips-TF, GLips-F, and GLips-TF were then stocked at 4 °C.

The Lips-P, Lips-TP, GLips-P, and GLips-TP were prepared in the similar approach except for the amount of PTX (10 mg) and TPTX (14 mg) added during the preparation.

2.7. *Entrapment efficiency (EE) and drug loading (DL) of liposomes*

To determine the PTX content in liposomes, the freshly prepared liposomes were firstly centrifuged at 10,000 rpm (LAB centrifuges, Beijing, China) for 5 min to remove the supernatant, and then methanol was added to dissolve the precipitation. The mixture solution was filtered through a microporous membrane with an aperture of 0.22 μm. The concentration of PTX was then detected using the RP-HPLC with a Thermo BDS HYPERSIL C18 reversed-phase chromatography column (150 mm × 4.6 mm, 5 μm) and a UV detector set at 227 nm. A mobile phase of methanol/water (70/30, *v*/*v*) was used with the flow rate set at 0.8 mL/min (35 °C).

The concentrations of PTX and TPTX were determined by comparing the peak areas with the standard curve. The entrapment efficiency (EE) and drug loading (DL) of normalized PTX were calculated according to the Eqs. (1) and (2) [23]:

$$EE\ (\%) = [\text{Weight of drug in liposomes/Weight of drug added}] \times 100 \quad (1)$$

$$DL\ (\%) = [\text{Weight of drug in liposomes/Weight of the formulation}] \times 100 \quad (2)$$

2.8. *The preparation of mixed liposomes and in vitro drug release*

The contents of FR and TFR encapsulated in liposomes were detected by fluorescence spectrophotometry and normalized. Before use, Lips-F was mixed with Lips-TF and GLips-F was mixed with GLips-TF in different ratios, and then allowed to stand for 30 min to obtain Lips-F/TF and GLips-F/TF with ratios of 1:0, 3:1, 1:1, 1:3, and 0:1. Detected by RP-HPLC method, the concentrations of Lips-P, Lips-TP, GLips-P, and GLips-TP were also normalized and mixed to obtain Lips-P/TP and GLips-P/TP with ratios of 1:0, 3:1, 1:1, 1:3, and 0:1.

The release of PTX and TPTX from liposomes was investigated using a dialysis method[20,22]. 1 mL liposomes were dispersed in 9 mL phosphate-buffered saline (PBS) and placed in a dialysis bag with molecular weight cut off 2000 Da. To investigate drug release behaviors in both neutral and acidic conditions, PBS solutions containing Tween 80 (0.1%, *w*/*v*) at different pH values (pH = 7.4, 6.8, and 5.5) were employed as the release media. The PBS solutions were stirred at 200 rpm (LAB centrifuges, Beijing, China) at 37 °C. At predetermined time intervals, 200 μL aliquots of release medium were withdrawn, and the same volume of fresh medium was added. *In vitro* release behaviors of PTX and TPTX from GLips-P/TP 1:0, GLips-P/TP 3:1, and GLips-P/TP 0:1 were detected by RP-HPLC analysis and the results were normalized into PTX release percentage. All assays were performed in triplicate.

2.9. *Cell culture and cellular uptake mechanism*

HeLa, L02, and HepG2 cells was purchased from the China Center for Type Culture Collection (Shanghai, China). They were cultured at 37 °C under a humid 5% CO_2 atmosphere in cell plates using Dulbecco's modified Eagle's medium (DMEM) with 10% fetal bovine serum (FBS) for 24 h until they reached 80% confluence.

HepG2 cells were seeded in cell culture dishes for 24 h to reach a confluence of 80%. The media were removed, and cells were washed with PBS twice. After incubation with cell culture media containing chlorpromazine (10 μg/mL), genistein (200 μg/mL), and wortmannin (50 nmol/L) for 1 h each, cells were further incubated with Gal (1.34%)-Lips-F at a fluorescein dose of 7.5 μg/mL for another 4 and 12 h. The excess medium was removed, and cells were washed with PBS trice, trypsinized and

centrifuged. The intracellular fluorescence intensity was detected by flow cytometer ($n = 3$).

2.10. Cellular imaging of FR, TFR, and their encapsulated mixed liposomes

L02 or HepG2 cells were seeded in cell culture dishes and incubated for 24 h. The FR, TFR, and FR/TFR-encapsulated liposomes (containing equivalent of 0.15 mmol/L FR) were diluted by cell culture medium was added to cell culture plates. Excess medium was removed after the incubation of 12 h. The cells were washed with PBS, and then MitoTracker® Red CMXRos (200 mmol/L) was added into the dishes and incubated for 30 min. The cells were washed with PBS for five times, and Hoechst 33,342 (5 μg/mL) was added into the dishes and incubated for 30 min. After the cells were washed with PBS for 5 times, pure PBS was added into the dishes for confocal laser scanning microscopy (CLSM) imaging.

2.11. Cytotoxicity and apoptosis

For the cytotoxicity assay, L02 cells and HepG2 cells were seeded in a 96-well plate (1.2×10^4 cells/well) and incubated in a growth medium with 5% FBS containing different concentrations of hybrid liposome samples for 24 h. After washing twice with 200 μL of PBS, the cell inhibition rates were detected using 3-(4,5-dimethylthiazol-2-yl)-2,5-diphenyl-tetrazoliumbromide (MTT, YEASEN, Shanghai, China) by comparing the absorbance at 490 nm with control wells containing only the cell culture medium. The data are presented as the means ± SD ($n = 3$), with each experiment repeated three times. The concentration of PTX that inhibited 50% cell growth compared to untreated cells (IC_{50}) was defined by curve fitting (LOGIT method) using SPSS 18.0 software.

Cells were incubated with GLips-P/TP 1:0, Lips-P/TP 3:1, GLips-P/TP 3:1, and GLips-P/TP 0:1 at 0.1 μg/mL of PTX for 24 h and then treated with the Annexin V-FITC/PI apoptosis detection kit (YEASEN). Afterward, the percentage of apoptotic cells was analyzed by the FACSCalibur system (BD, Franklin, USA).

2.12. Caspase-3 and caspase-9 activities

L02 or HepG2 cells were cultured under 5% CO_2 at 37 °C for 12 h. Then cells were treated with PTX, TPTX, or GLips-P/TP liposomes (all equivalent of 1 μg/mL PTX) and incubated for 12 h. Control experiments were performed by adding culture medium. After 12 h incubation, cells were collected and washed with PBS and then cells were reacted with lysis buffer (provided in the kit) for 1 h in an ice bath. Then cell lysates were centrifuged at 10,000 rpm (LAB centrifuges) for 1 min. Supernatants were incubated with caspase-3 and caspase-9 substrates at 37 °C for 4 h in the dark. Caspase-3 and caspase-9 activities were measured at 405 nm with a microplate reader, and activity ratios were calculated according to the instruction of colorimetric assay kits (KeyGEN, Nanjing, China)[24,25].

2.13. In vivo antitumor efficacy

Healthy male ICR mice (20−25 g, Certificate number: SCXK (Su) 2012−0004) were purchased from the Comparative Medicine Centre of Yangzhou University (Yangzhou, China). Heps cells (Hepatoma solidity) were kindly provided by Nanjing University and were maintained as an ascites tumor in ICR mice. Heps cell suspensions containing 1×10^6 cells per 0.1 mL were implanted subcutaneously into the right axillary space. All the animals were pathogen free and were allowed free access to food and water. The experiments were carried out in compliance with the National Institute of Health Guide for the Care and Use of Laboratory Animals. The tumor-bearing mice were subjected to antitumor activity studies after the tumor volume reached 200 mm^3. Animals with a tumor after Heps tumor inoculation were divided into six groups: saline, Taxol, GLips-P/TP 1:0, Lips-P/TP 3:1, GLips-P/TP 3:1, GLips-P/TP 0:1. These formulations were diluted in saline. Tumor-bearing mice were injected through the tail vein with 20 mg/kg of PTX in the indicated formulation at 2-day intervals. Tumor volume was calculated by the Eq. (3):

$$\text{Tumor volume } (mm^3) = (\text{Length} \times \text{width}^2)/2 \quad (3)$$

At the end of the experiment, tumor tissues were excised, washed with saline, and weighed. The data were presented as the mean ± SD ($n = 5$). To evaluate the toxicity of the six formulations, the tumor-bearing mice in the survival rate experiment were also injected through the tail vein.

2.14. Histological analysis

The excised tumor tissues were fixed with 4% paraformaldehyde. The samples were processed and sectioned, and thin tissue sections were stained with hematoxylin and eosin (H&E) or TdT-mediated dUTP nick end labeling (TUNEL) using a TUNEL apoptosis detection kit (Beyotime Institute of Biotechnology, China). The H&E- or TUNEL-stained sections were observed using Eclipse CI and Eclipse TI-SR microscopes (Nikon Optical Co., Ltd., Japan), respectively.

2.15. Pharmacokinetics studies

Healthy male ICR mice (20 ± 2 g) were used to examine the pharmacokinetics of four liposome formulations and using Taxol as a reference. The mice were randomly divided into five groups ($n = 3$). Both Taxol and liposome samples were intravenously administered through the tail vein with an equivalent dose of 20 mg/kg of PTX. Blood samples (0.5 mL) were collected from the plexus venous at various times (0.5, 1, 4, 8, 12, and 24 h) into heparinized tubes. The plasma samples were collected after immediate centrifugation at 15,000 rpm (LAB centrifuges) for 10 min and stored at −20 °C until analysis. 0.1 mL aliquot of plasma was added to 0.2 mL of methanol to extract the PTX, and subjected to plasma protein precipitation by vigorous vortexing. After centrifugation at 15,000 rpm (LAB centrifuges) for 3 min, the supernatant was concentrated under vacuum. The residue was dissolved in 0.2 mL of mobile phase and centrifuged at 15,000 rpm (LAB centrifuges) for 3 min, and the supernatant was analyzed by RP-HPLC as described above.

2.16. Biodistribution

ICR male mice with a tumor volume of 200 mm^3 after Heps tumor inoculation were randomly divided into five groups. The test formulations including Taxol, GLips-P/TP 1:0, Lips-P/TPX 3:1, GLips-P/TP 3:1, GLips-P/TP 0:1 were injected intravenously

through the tail vein with equivalent dose of 20 mg/kg PTX. After administration, the mice were sacrificed at predetermined time points (0.5, 1, 4, 8, 12 and 24 h), and heart, liver, spleen, lung, kidney, and tumor tissues were collected and homogenized with 1 mL of saline, and 0.1 mL of the homogenate was added with 0.2 mL of methanol, vortexed and centrifuged at 15,000 rpm (LAB centrifuges) for 3 min. The supernatant was then analyzed by RP-HPLC as described above. The calibration curves of the tissues displayed good linearity.

2.17. *Statistical analysis*

All the results are presented as the mean ± SD. The data were analyzed by one-way analysis of variance (ANOVA) with the appropriate Bonferroni correction to determine significant differences for multiple comparisons. $^{*}P < 0.05$ and $^{**}P < 0.01$ were statistically significant and very significant.

3. Results and discussion

3.1. *Preparation, characterization, and liver tumor cell targeting of GLips*

To achieve the solid tumor targeting of chemical drugs *via* enhanced permeability and retention effect, liposome was employed as a model nanocarrier (Fig. 2A) to construct the cascade targeting delivery system. Based on the previous reports, galactose modified carriers show selective recognition and specific binding with highly expressed asialoglycoprotein receptor (ASGP-R) on the surface of hepatic carcinoma (HepG2) cells[26–28], providing useful means for targeted chemotherapy of liver cancer. The galactose on the surface of the carriers could largely improve tumor cell uptake of the drug carriers, and the targeting efficiency is dependent on the density of galactose exposed on the surface of carriers[29]. Here, to realize liver tumor targeting, lactobionic acid (LA) containing galactose moiety is connected on the hydrophilic end of DSPE-PEG-NH_2 *via* the amidation reaction between LA and DSPE-PEG-NH_2 (Fig. 2B). The synthesis procedure of DSPE-PEG-LA was described in Experimental Section and its chemical structure was characterized by FT-IR and ^{1}H NMR (Supporting Information Fig. S1).

The DSPE-PEG-LA was doped in the structure of Lips, in different ratios *versus* unmodified DSPE-PEG using a thin-film dispersion method[21,22], to obtain GLips. The galactose density on the surface of GLips enhanced with the increasing amount of DSPE-PEG-LA added in the preparation solutions. Finally, the galactose density of 0.67%, 1.34%, and 2.68% in the molar percentage of DSPE-PEG-LA in liposomes were obtained, respectively. For revealing the targeting ability of GLips, FR with green fluorescence, was employed as a model drug and encapsulated in GLips. The hydrodynamic diameters of GLips-F with different galactose modification are measured by dynamic light scattering (DLS) method, which are ∼115 nm and show no significant difference (Fig. 2C). The liposome morphologies are observed spherical and displayed a good dispersity through TEM micrographs (Fig. 2D). The zeta potential of the Lips-F is around −42 mV, the most negatively charged liposome due to the negative charge of soya phosphatidyl choline. After the addition of DSPE-PEG-LA, the surface negativity was reduced because of the neutral long chains of PEG and the galactose ligands. Although zeta potentials decreased with the increase of galactose density, changing from -10.5 ± 4.2 mV, -17.95 ± 3.3 mV, to -25.38 ± 5.4 mV for GLips(0.67%)-F, GLips(1.34%)-F, and GLips(2.68%)-F, respectively, there are no significant difference between these samples (Fig. 2E). The GLips(1.34%)-F in the middle galactose density was used to investigate the cell selectivity among different cell lines, *e.g.*, human cervical cancer cells (HeLa), human normal liver cells (L02), and HepG2, which express no, low, and high level of ASGP-R, respectively. After the incubation for 12 h, semi-quantitative flow cytometry was employed to detect the intracellular fluorescence intensity of FR in different cells. Compared with Lips-F, GLips-F with galactose modification showed the highest uptake of FR in HepG2 cells (Fig. 2F), confirming its liver tumor cell specificity. Moreover, the cellular uptake of GLips with different galactose density against HepG2 cells was also detected (Fig. 2G). Glips(1.34%)-F showed the best targeting ability than other two groups, and thus we used GLips of 1.34% galactose density in the following studies.

3.2. *Synthesis, characterization, and mitochondria targeting of TPP-modified molecule*

Covalent attachment of TPP has become a robust method for selectively delivering small and bioactive molecules to mitochondria[30–32]. In order to deliver the model drug, FR, to mitochondria, 5-aminofluorescein (5-AFR) was coupled to TPP-COOH *via* an amidation reaction to give TFR (Fig. 3A and B). The synthesis procedure of TFR was described in Experimental Section and its chemical structure was characterized by FT-IR and ^{1}H NMR spectroscopies (Supporting Information Fig. S2). After covalently attached by TPP, even though there are some changes in UV−vis spectra of TFR *versus* FR, the fluorescence emission spectrum of TFR showed no significant difference to that of FR under an equimolar concentration condition (Supporting Information Fig. S3). Therefore, the intracellular distribution of TFR in HepG2 cells was monitored by CLSM.

TFR fully lighted up whole cell and showed a brighter fluorescence intensity compared with FR (Fig. 3C). It indicates that the positively charged TPP moiety has higher membrane penetration that facilitates the cellular uptake of the modified FR as well as its distribution in membranous organelles such as nucleus and mitochondria. To compare the organelle distribution of these two probes, nucleus and mitochondria were separated from HepG2 cells using commercial organelle separation kits and detected by the flow cytometry method (Fig. 3D). The TFR group showed a higher fluorescence intensity in mitochondria (10.3%) than in nucleus (1.1%) in comparison with FR (6.0% in mitochondria and 2.1% in nucleus), demonstrating the mitochondria targeting ability of TPP-modified molecules.

3.3. *Preparation of mixed liposomes and their intracellular distribution*

Either FR or TFR was loaded in Lips and GLips, denoted as Lips-F, Lips-TF, GLips-F, and GLips-TF. The molar concentration of FR and TFR in these liposomes was optimized and normalized. Liposomes prepared above were mixed in different volumes of 1:0, 3:1, 1:1, 1:3, and 0:1 as showed in Fig. 4, named as Lips-F/TF and GLips-F/TF. Hydrodynamic diameters (Supporting Information Figs. S4A and B) and zeta potentials (Figs. S4C and D) of mixed liposomes were detected in 30 min after mixing, which showed no dramatic changes in 30 min, indicating no fusion and reconstruction of liposomes occurred in the mixed solutions[33]. From TEM micrographs, the mixed liposomes kept

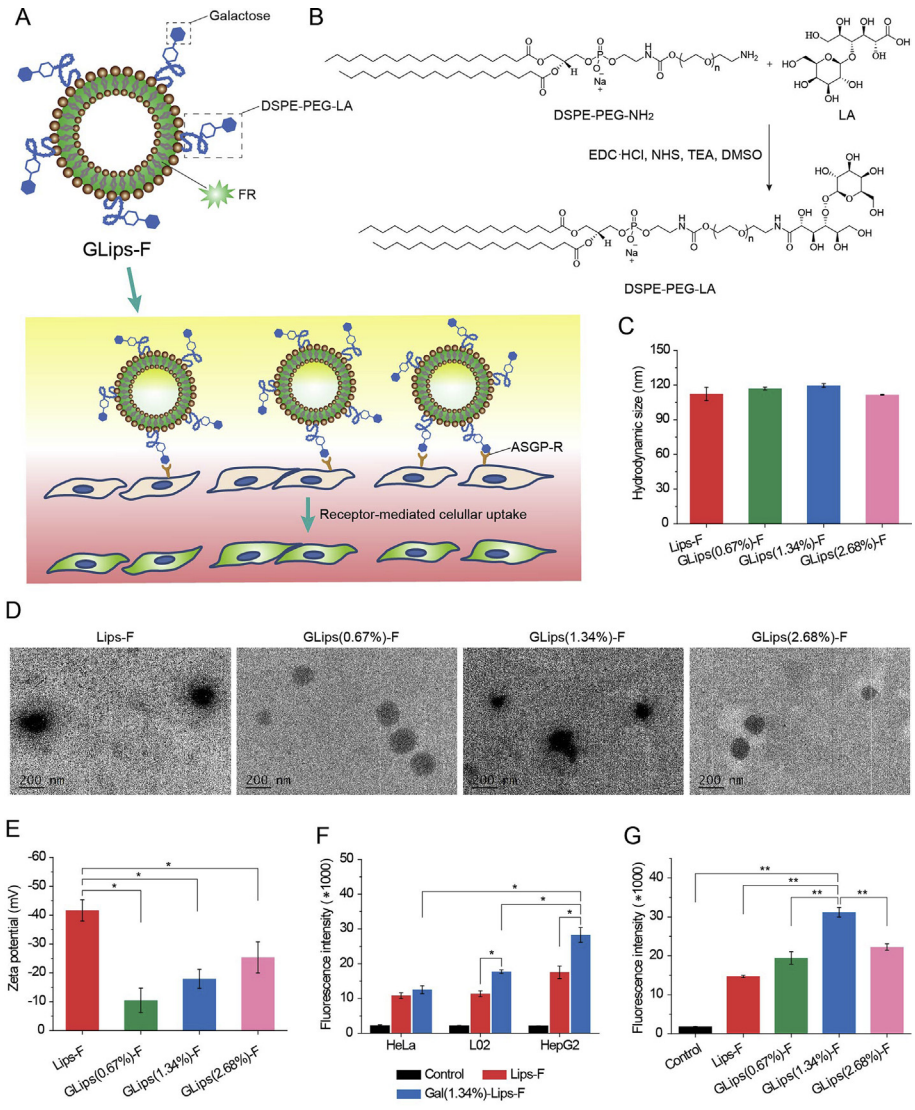

Figure 2 Liver targeting of GLips. (A) The structure illustration of ASGP-R targeting liposomes and their receptor-mediated cellular uptake. (B) The synthesis procedure of DSPE-PEG-LA. (C) Hydrodynamic diameters, (D) transmission electron microscope (TEM) images, (E) zeta potentials of GLips-F with different galactose density (Lips-F without LA modification is used as the control). Cellular uptake of FR-loaded liposomes (containing 0.0075 mmol/L FR) (F) with the same LA modification (Gal 1.34%) in different cell lines, including HeLa, L02, and HepG2 cells and (G) with different LA modification (Gal 0.67%, 1.34%, and 2.68%) in HepG2. The data present the mean ± SD ($n = 3$). $^{*}P < 0.05$, $^{**}P < 0.01$ (one-sample t-test).

well-dispersed morphologies and demonstrated a steady state (Fig. S4E).

To reveal the cellular uptake mechanism of galactose-modified liposomes, the uptake of GLips-F in the absence and presence of chlorpromazine, genistein, and wortmannin, the inhibitors for clathrin-mediated endocytosis, membrane cave-like depression-mediated endocytosis, and macropinocytosis, respectively, was detected and showed in Supporting Information Fig. S5. HepG2 cells preincubated with wortmannin displayed significant inhibition of cellular uptake at both 4 and 12 h, which indicated that macropinocytosis was the main uptake mechanism of GLips-F.

To investigate the intracellular distribution of FR-related molecules, HepG2 cells were monitored using CLSM after the incubation of various mixed liposomes for 12 h (Supporting Information Fig. S6) and the fluorescence intensity in mitochondria was detected using flow cytometry assay (Fig. 4). It was noting that the galactose decoration on liposomes would increase the fluorescence intensity in HepG2 cells and the increase of TFR proportion was the major factor that increased the distribution of probe molecules in mitochondria. Thus, we can draw a conclusion that the galactose modification on liposomes mainly took charge of cell targeting of liver cancer, while TPP-moiety was responsible for mitochondrial selectivity inside cells. All results described above demonstrated the cascade targeting ability of drug in mixed liposomes.

3.4. *In vitro drug release and cytotoxicity of mixed liposomes*

To construct the cascade targeting system using a chemical drug and evaluate its combinatory treatment efficiency, PTX was used instead of FR in above mixed liposomes. TPTX, the TPP

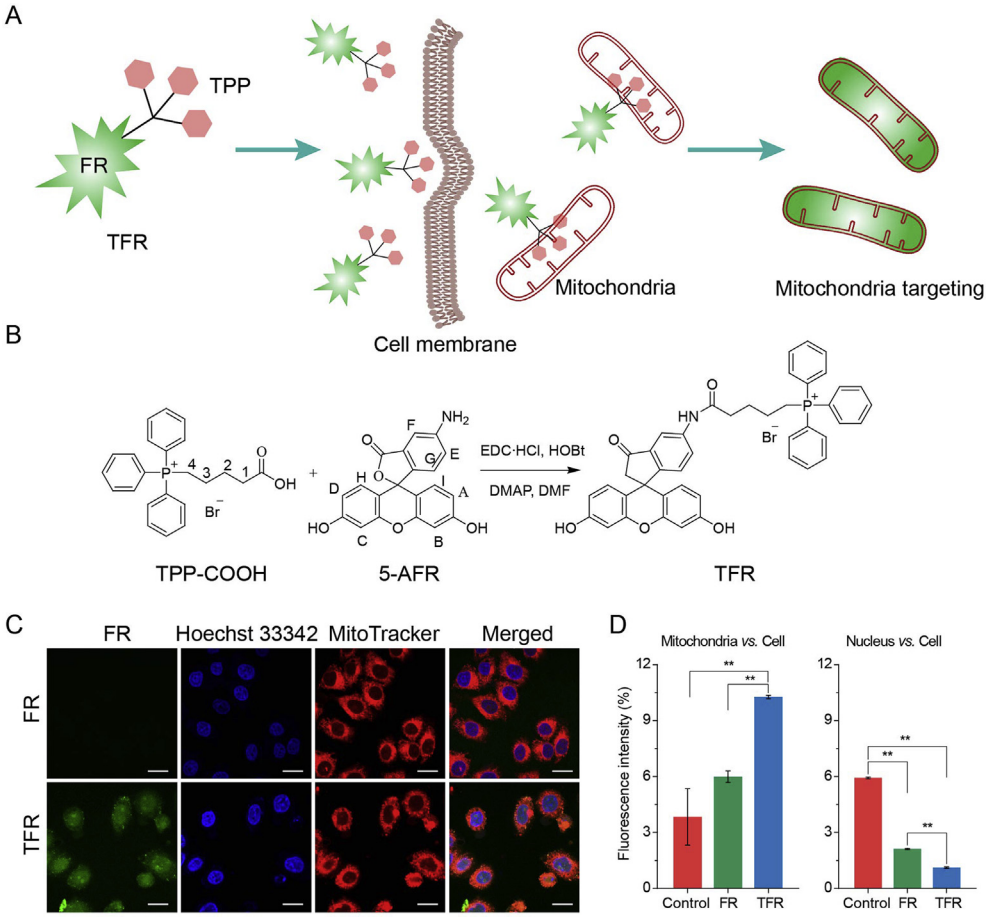

Figure 3 Mitochondria targeting of TFR. (A) The illustration of the structure of TFR and its cell membrane permeability and mitochondrial targeting. (B) The synthesis procedure of TFR. (C) CLSM images of HepG2 cells after incubated with FR and TFR (0.15 mmol/L) at 37 °C for 12 h, respectively, and the nuclei were stained by Hoechst 33,342. The scale bar is 20 μm. (D) Intracellular distribution of FR and TFR in mitochondria and nucleus *vs.* cell, respectively, detected by the flow cytometry. Cells without incubation of FR or TFR were used as control. The data present the mean ± SD ($n = 3$). $^{*}P < 0.05$, $^{**}P < 0.01$ (one-sample *t*-test).

derivative of PTX, was synthesized and characterized by FT-IR and ^{1}H NMR spectra (Supporting Information Fig. S7). According to the same method, either PTX or TPTX was loaded in Lips and GLips (1.34%), named as Lips-P, Lips-TP, GLips-P, and GLips-TP, and the drug loading and entrapment efficiency of GLips-P and GLips-TP were showed in Supporting Information Fig. S8. After normalizing the drug molar concentrations of PTX and TPTX in these liposomes that were mixed in different volumes, Lips-P/TP and GLips-P/TP were obtained based on similar approach shown in Fig. 4. The hydrodynamic sizes and zeta potentials of Lips-P/TP and GLips-P/TP were showed in Supporting Information Fig. S9. The release profiles of normalized PTX from liposomes with different PTX *vs.* TPTX ratios exhibited that the total drug release was more rapid in acidic media than those in neutral media (Supporting Information Fig. S10), which was desirable to the selective drug release at the tumor site.

The combined effect of the mixed liposomes was evaluated by MTT assay. The cell viability of two series of mixed liposomes was presented in Fig. 5A−D after a 24 h incubation with L02 and HepG2 cells, respectively. The IC_{50} and the combination index (CI) values[34] of all test groups were listed in Table 1. Compared to the single drug groups and mixed liposomes with other ratios, the highest cell inhibition was occurred in the galactose-modified group when the molar ratio of PTX:TPTX was 3:1 ($IC_{50} = 0.09 \pm 0.01$ μg/mL) against HepG2 cells. It was noting that, for the same formulation, GLips-P/TP 3:1 also showed the lowest CI value (*i.e.*, 0.28) among all test groups, indicating that the best beneficial synergistic effect. These results demonstrated that (1) galactose-modified liposomes offer the loaded drugs higher cytotoxicity against HepG2 cells; (2) both PTX and TPTX play their own roles *via* different mechanisms, respectively, and show synergistic effects; and (3) the inhibition of tumor cells is mainly based on the interaction between PTX and tubulins (IC_{50} GLips-P/TP 1:0 $= 0.26 \pm 0.03$ μg/mL *vs.* IC_{50} Lips-P/TP 0:1 $= 1.56 \pm 0.33$ μg/mL), which has been previously proved[28,35−37].

3.5. *Caspase activity and apoptosis*

Caspases are a group of cysteine proteases existing in cytoplasmic sol, play critical roles in the initiation and execution of apoptosis[24,38]. Cumulative oxidative stress with disrupted mitochondrial respiration and mitochondrial damage by chemical drugs will lead to the release of cytochrome *c* (Cyt *c*) from mitochondria into the cytosol[39,40]. A Cyt *c*-bound adaptor protein (APAF-1) recruits initiator caspase-9 to form apoptosome, *i.e.*, a

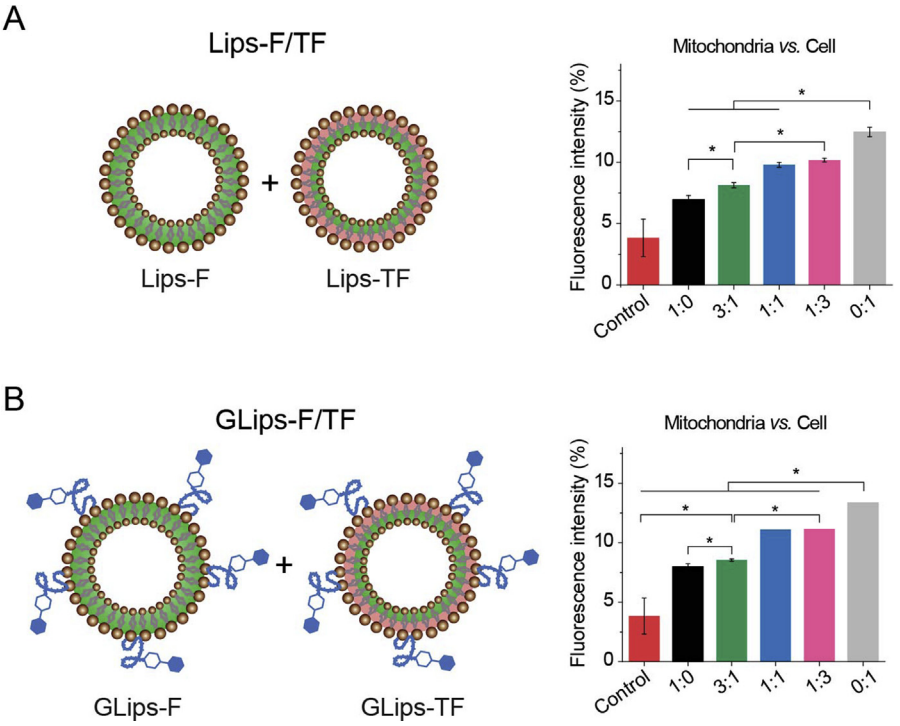

Figure 4 Intracellular distribution of FR and TFR-encapsulated mixed liposomes, (A) Lips-F/TF and (B) GLips-F/TF, in mitochondria *vs.* cell, respectively, detected by the flow cytometry. The data present the mean ± SD ($n = 3$). $^{*}P < 0.05$, $^{**}P < 0.01$ (one-sample *t*-test).

caspase activating multiprotein complex. Once activated, initiator caspases such as caspase-9 will cleave and activate other executioner caspases. This leads to degradation of cellular components for apoptosis. There are 13 known species, including caspase-3 and caspase-9 that have similar substrate and inhibitor specificities, have been identified as the well-established cellular markers of apoptosis[25,41].

To further validate the mitochondria-mediated mechanism of TPTX, the activities of caspase-3 and caspase-9 initiated by TPTX-containing formulations were detected in L02 and HepG2 cells (Fig. 6A−D). Comparing with PTX, TPTX increased the activities of both caspase-3 and caspase-9 in test cells, especially for HepG2 cells, about 1.4-fold of those treated with the same dose of PTX (Fig. 6B). Among all test liposomes, GLips-P/TP 0:1

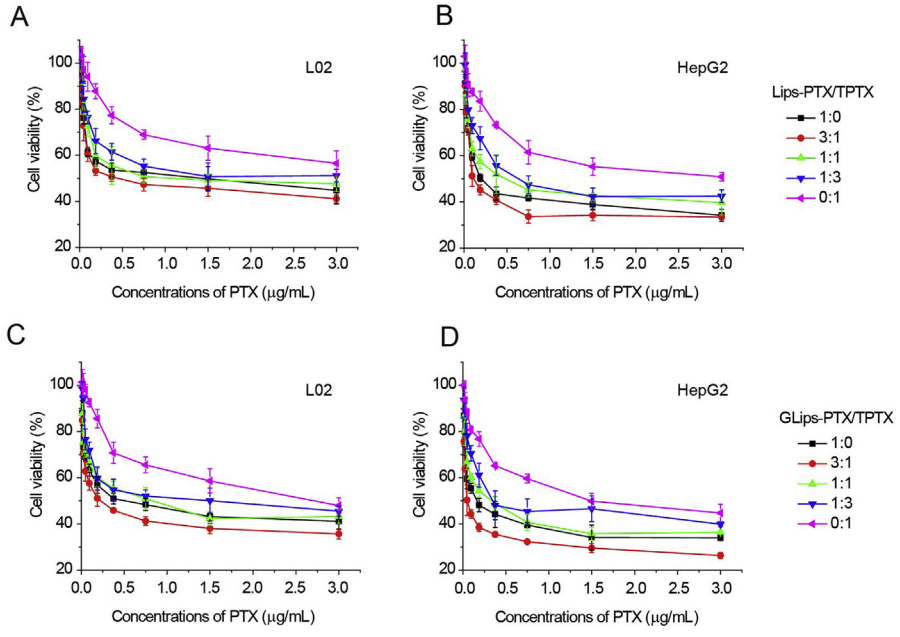

Figure 5 Cell viability of (A, C) L02 cells and (B, D) HepG2 cells after incubating with (A, B) Lips-P/TP and (C, D) GLips-P/TP at the same dose of PTX for 24 h.

Table 1 IC_{50} and CI values of mixed liposomes in L02 and HepG2 cells (μg/mL, mean ± SD, $n = 3$).

Molar ratio	L02 cells				HepG2 cells			
	Lips-P/TP		GLips-P/TP		Lips-P/TP		GLips-P/TP	
	IC_{50} (μg/mL)	CI	IC_{50} (μg/mL)	CI	IC_{50} (μg/mL)	CI	IC_{50} (μg/mL)	CI
1:0	0.97±0.23	–	0.63±0.10*	–	0.37±0 0.04**	–	0.26±0.03**	–
3:1	0.63±0.06	0.69	0.32±0.015**	0.48	0.26±0.01**	0.61	0.09±0.01**	0.28
1:1	1.06±0.17	0.74	0.81±0.16	0.96	0.62±0.04**	1.06	0.40±0.03**	0.95
1:3	1.71±0.32	0.95	1.07±0.24**	0.99	0.79±0.19**	1.10	0.71±0.06**	1.25
0:1	3.66±1.14	–	2.17±0.16*	–	2.35±0.40*	–	1.56±0.33**	–

$^{*}P < 0.05$, $^{**}P < 0.01$ *vs.* Lips-P/TP (one-sample *t*-test). –Not applicable.

caused the highest caspase-3 and caspase-9 activities that was a 2-fold higher than the control (Fig. 6D). It confirmed the obvious interference with mitochondria by TPTX.

Thus, to evaluate the contribution of TPTX in the growth inhibition of tumor cells, cellular apoptosis of GLips-P/TP 3:1 was detected using Annexin V-FITC/PI staining and flow cytometry method (Fig. 6E and F). GLips-P/TP 1:0, Lips-P/TP 3:1, and GLips-P/TP 0:1 were used as the controls. Four formulations have similar late apoptosis rate towards L02 cells (Fig. 6E), but the apoptosis rates against sensitive HepG2 cells were different (Fig. 6F). It was also found that, when PTX caused serious cellular apoptosis (GLips-P/TP 1:0, 36.5%), TPTX also played an important role through the mitochondria-mediated pathway (GLips-P/TP 0:1, 21.0%). However, it was worth noting that, the

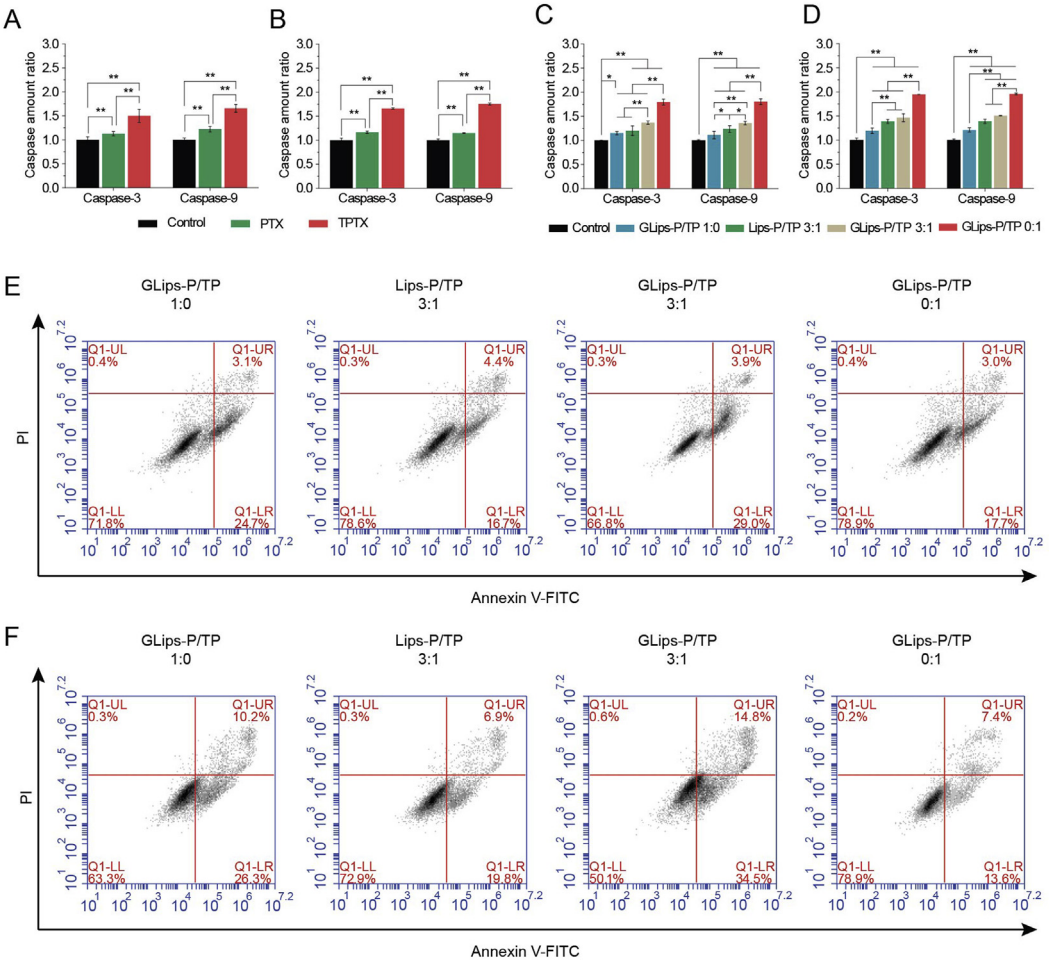

Figure 6 Caspase-3 and caspase-9 amounts in (A, C) L02 cells and (B, D) HepG2 cells after incubating with culture medium (control), PTX, TPTX, and mixed liposome formulations at the same dose of PTX (1 μg/mL) for 12 h. Data represents mean ± SD, $n = 3$. $^{*}P < 0.05$, $^{**}P < 0.01$, one-sample *t*-test. Apoptosis of (E) L02 and (F) HepG2 cells after the incubation with GLips-P/TP 1:0, Lips-P/TP 3:1, GLips-P/TP 3:1, and GLips-P/TP 0:1 with the same dose of PTX for 24 h using annexin V-FITC/PI staining. In each panel, the lower-left (annexin V-FITC^{-}, PI^{-}), lower-right (annexin V-FITC^{+}, PI^{-}) and upper-right (annexin V-FITC^{+}, PI^{+}) quadrants represent the populations of live cells, early apoptotic cells, and late apoptotic cells, respectively. The average population (%) in each quadrant is indicated by numbers at the corner of the panels.

percentage of apoptotic cells in GLips-P/TP 3:1 treated group (49.3%) was the highest, nearly 1.4-, 1.8-, and 2.3-fold higher than GLips-P/TP 1:0, Lips-P/TP 3:1 (26.7%), and GLips-P/TP 0:1 treated groups, respectively (Fig. 6F). It means that, when 25% PTX was changed into TPTX in mixed liposomes, *e.g.*, GLips-P/TP 3:1, the contribution of auxiliary therapeutic mechanism related to mitochondria was enhanced and showed the drug synergy even though only one drug was used.

3.6. *Pharmacokinetics, in vivo antitumor efficiency, and biodistribution*

To evaluate the capability of long circulation *in vivo* for test formulations, after i.v. administration of Taxol® and mixed liposomes in mice, the plasma PTX concentration−time profiles were detected using RP-HPLC method (Supporting Information Fig. S11). All liposomes have higher plasma concentrations of PTX from 0 to 12 h compared to Taxol®, indicating the protection effect of liposome carrier on the stability of chemical drug. Although the pharmacokinetic characters of mixed liposomes showed no significant difference, which can be found both from the profiles (Fig. S11A) and the pharmacokinetic parameters listed in the table (Fig. S11B), GLips-P/TP 3:1 showed the highest $t_{1/2}$ and AUC values. It could be due to the polysaccharide-like surface of modified liposomes, which was found offering long-time circulation property to drug carriers in our previous work and other literature[28,29,42]. This desirable long circulation property of GLips-P/TP 3:1 would improve its probability to enter tumors, and then subsequently enhance the accumulation and internalization in liver tumor cells *via* the specific recognition between galactose moiety and ASGP-R.

To prove our hypothesis, *in vivo* antitumor efficiency studies were also carried out in Institute of Cancer Research (ICR) mice bearing Heps tumors (Fig. 7). Compared to saline, Taxol® and other liposomes, GLips-P/TP 3:1 suppressed the tumor growth from the 2nd day (Fig. 7A) and showed the lowest tumor size and weight after 10-day treatment (Fig. 7B and C). The relative tumor volume and weight on the 10th day in GLips-P/TP 3:1 treated group ($V/V_0 = 4.5 \pm 0.6$ and 0.22 ± 0.5 g) was much lower than those of GLips-P/TP 1:0 ($V/V_0 = 7.4 \pm 1.7$ and 0.5 ± 0.1 g) and GLips-p/TP 0:1 ($V/V_0 = 9.0 \pm 1.6$ and 0.8 ± 0.2 g), demonstrating the synergistic treatment of PTX and TPTX in this combined therapy system. In addition, there were no significant differences in body weight among all test groups (Fig. 7D),

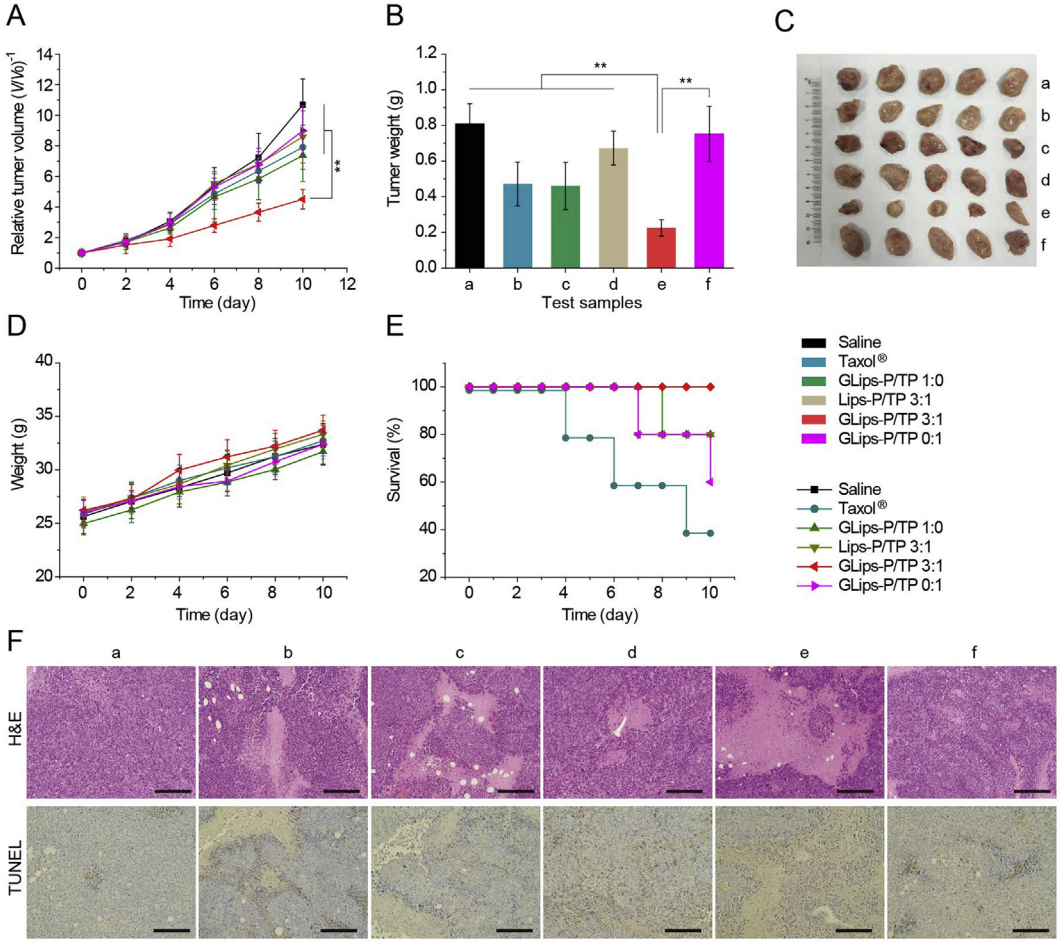

Figure 7 *In vivo* antitumor efficacy. (A) Relative tumor volume, (B) tumor weight, (C) the photograph of typical tumors 10 days post-injection, (D) body weight, and (E) survival rates of Heps tumor xenograft ICR mouse models after intravenous injection of (a) saline, (b) Taxol®, (c) GLips-P/TP 1:0, (d) Lips-P/TP 3:1, (e) GLips-P/TP 3:1, and (f) GLips-P/TP 0:1 at a PTX dose of 20 mg/kg. Each point in (A), (B), (D), and (E) represents the mean ± SD ($n = 5$). $^{*}P < 0.05$, $^{**}P < 0.01$, one-sample *t*-test. (F) Histological observation of tumor tissue sections (stained with H&E) and detection of apoptosis in tumor tissue sections (stained by TdT-mediated dUTP nick end labelling using a TdT-mediated dUTP nick end labeling (TUNEL) kit, Beyotime Institute of Biotechnology, China) from control and test groups 10 days post-injection. The scale bar is 200 μm.

although the control groups showed a rapid growth in tumor size and weight, implying the mice in the GLips-P/TP 3:1 group led a high quality of life. This result was also reflected from the highest survival rate of the GLips-P/TP 3:1 treated group (Figs. 7E), 100% in the whole treatment duration while the survival rates of the saline and Taxol® groups were only 80% and 60%, respectively. The improved treatment efficacy and biosafety of GLips-P/TP 3:1 confirmed that the combination therapy can be achieved by one single drug.

This high therapeutic efficacy and biosafety can be due to the precise accumulation of drug in tumor tissues and its unique cascade targeting delivery. Therefore, the biodistribution and the histological observation of tumor and normal tissues have been carried out. The normalized PTX concentrations in the tumor and normal tissues, including heart, liver, spleen, lung, and kidney, of Heps heterotopic xenografts tumor models treated with different formulations were detected and are shown in Fig. S12. In tumor tissues, PTX concentrations in Taxol® group decreased rapidly in the 24 h (Fig. S12F). This result can be explained by the rapid drug distribution of free PTX in the whole body and subsequent quick elimination from the circulation. Compare to Taxol®, intratumoral PTX concentrations for four groups of liposome formulations increased firstly and decreased slowly, exhibiting prolonged retention time in tumor tissue, especially for those galactose-modified liposomes, *e.g.*, GLips-P/TP 1:0, 3:1, and 0:1. Among them, GLips-P/TP 3:1 showed the highest PTX levels in tumors from 0.5 to 24 h, reaching a maximum at 4 h (32.92 ± 1.75 μg/g). This effective accumulation in tumor tissues caused the maximum area of necrosis of H&E stained tumor tissue sections at 10-day post-injection (Fig. 7F, group e). However, the degree of apoptosis in the tumor tissue of GLips-P/TP 3:1 group was lower than GLips-P/TP 0:1 (Fig. 7F), confirming the mitochondria-related apoptosis was one of the reasons for tumor cell death. Moreover, to evaluate the biosafety of hybrid liposomes, the biodistribution of PTX in normal tissues and their histological examination of H&E and TUNEL stained sections were also detected. As shown in Figs. S10A−E, liposome formulations showed lower distribution in heart and liver than Taxol® and didn't display higher accumulation in all normal tissues especially after 8 h. Furthermore, no obvious impairment and apoptosis is found in liposome-treated normal tissues stained by H&E and TUNEL (Supporting Information Fig. S13), proving the biosafety of liposome preparations.

4. Conclusions

Improving the treatment efficacy and biosafety of antitumor drugs are the eternal theme of chemotherapy. The former can be solved by combination therapy, the latter requires the precise target delivery of chemical drugs into lesions. In this work, an optimized mixed liposome loading PTX and its TPP derivative was constructed. This simple system showed multi-advantages that both solved the main issues in combination therapy and improved the specificity of drug in tumor. Instead of multi-drugs, using one single drug simplified the structure, clarified the mechanism, and improved the controllability of the combined therapy system. The designed mixed liposomes featuring cascade "tissue-cell-organelle" targeting function that precisely deliver PTX and TPTX to cytoplasm and mitochondria, respectively, which was responsible for binding microtubules in cytoplasm and releasing cytochrome *c* from mitochondria. Finally, the dose control of drugs was finely controlled by simply mixing the liposomes in different ratio; the synergistic treatment was enhanced by combining the primary and secondary mechanism of one drug; the treatment efficacy and biosafety in liver cancer therapy were significantly improved.

Acknowledgments

This work was supported by grants from the National Natural Science Foundation of China (31870946, 31470916 and 51672010), the Funding of Double First-rate discipline construction (CPU2018GF07, China), the Priority Academic Program Development of Jiangsu Higher Education Institutions, and the Open Project Program of MOE Key Laboratory of Drug Quality Control and Pharmacovigilance (DQCP2015MS01, China).

Author contributions

Aiyun Liu, Xiaoshuang Hou, and Yu Ma designed and performed the experiments, and analysed the data. Huaisong Wang, Gongjun Yang, and Yanglong Hou. analysed and interpreted the data, and wrote the manuscript. Ya Ding conceived and supervised the project, and analysed and interpreted the data. All the authors discussed the results and reviewed the manuscript.

Conflicts of interest

The authors have no conflicts of interest to declare.

Appendix A. Supporting information

Supporting data to this article can be found online at https://doi.org/10.1016/j.apsb.2019.08.011.

References

1. Mei D, Chen B, He B, Liu H, Lin Z, Lin J, et al. Actively priming autophagic cell death with novel transferrin receptor-targeted nanomedicine for synergistic chemotherapy against breast cancer. *Acta Pharm Sin B* 2019;**9**:1061−77.
2. Hu Q, Sun W, Wang C, Gu Z. Recent advances of cocktail chemotherapy by combination drug delivery systems. *Adv Drug Deliv Rev* 2015;**98**:19−34.
3. Parhi P, Mohanty C, Sahoo SK. Nanotechnology-based combinational drug delivery: an emerging approach for cancer therapy. *Drug Discov Today* 2012;**17**:1044−52.
4. Kang L, Gao Z, Huang W, Jin M, Wang Q. Nanocarrier-mediated co-delivery of chemotherapeutic drugs and gene agents for cancer treatment. *Acta Pharm Sin B* 2015;**5**:169−75.
5. Miao L, Guo S, Lin CM, Liu Q, Huang L. Nanoformulations for combination or cascade anticancer therapy. *Adv Drug Deliv Rev* 2017;**115**:3−22.
6. Marupudi NI, Han JE, Li KW, Renard VM, Tyler BM, Brem H. Paclitaxel: a review of adverse toxicities and novel delivery strategies. *Expert Opin Drug Saf* 2007;**6**:609−21.
7. Tacar O, Sriamornsak P, Dass CR. Doxorubicin: an update on anticancer molecular action, toxicity and novel drug delivery systems. *J Pharm Pharmacol* 2012;**65**:157−70.
8. Kunnumakkara AB, Anand P, Aggarwal BB. Curcumin inhibits proliferation, invasion, angiogenesis and metastasis of different cancers through interaction with multiple cell signaling proteins. *Cancer Lett* 2008;**269**:199−225.
9. Dong LF, Jameson VJA, Tilly D D, Prochazka L, Rohlena J, Valis K, et al. Mitochondrial targeting of α-tocopheryl succinate enhances its

pro-apoptotic efficacy: a new paradigm for effective cancer therapy. *Free Radical Biol Med* 2011;**50**:1546−55.
10. Fan W. Possible mechanisms of paclitaxel-induced apoptosis. *Biochem Pharmacol* 1999;**57**:1215−21.
11. Wang TH, Wang HS, Soong YS. Paclitaxel-induced cell death: where the cell cycle and apoptosis come together. *Cancer* 2000;**88**:2619−28.
12. André N, Braguer D, Brasseur G, Gonçalves A, Lemesle-Meunier D, Guise S, et al. Paclitaxel induces release of cytochrome *c* from mitochondria isolated from human neuroblastoma cells. *Cancer Res* 2000;**60**:5349−53.
13. Barranco SC, Gerner EW, Burk KH, Humphrey RM. Survival and cell kineticseffects of adriamycin on mammalian cells. *Cancer Res* 1973;**33**:11−6.
14. Ewa CS, Sławomir W, Milena D, Janusz D, Tomasz A. The effect of doxorubicin and retinoids on proliferation, necrosis and apoptosis in MCF-7 breast cancer cells. *Folia Histochem Cyto* 2004;**42**:221−7.
15. Xu TT, Li JH, Cheng FR, Zhang YX, Cao J, Gao WX, et al. Fabrication of a polypseudorotaxane nanoparticle with synergistic photodynamic and chemotherapy. *Chin Chem Lett* 2017;**28**:1885−8.
16. Granados-Principal S, El-azem N, Pamplona R, Ramirez-Tortosa C, Pulido-Moran M, Vera-Ramirez L, et al. Hydroxytyrosol ameliorates oxidative stress and mitochondrial dysfunction in doxorubicin-induced cardiotoxicity in rats with breast cancer. *Biochem Pharmacol* 2014;**90**:25−33.
17. D'Souza GG, Wagle MA, Saxena V, Shah A. Approaches for targeting mitochondria in cancer therapy. *Biochim Biophys Acta* 2011;**1807**:689−96.
18. Heller A, Brockhoff G, Goepferich A. Targeting drugs to mitochondria. *Eur J Pharm Biopharm* 2012;**82**:1−18.
19. Wenner CE. Targeting mitochondria as a therapeutic target in cancer. *J Cell Physiol* 2012;**227**:450−6.
20. Ding Y, Zhou YY, Chen H, Geng DD, Wu DY, Hong J, et al. The performance of thiol-terminated PEG-paclitaxel-conjugated gold nanoparticles. *Biomaterials* 2013;**34**:10217−27.
21. Liu D, Liu F, Liu Z, Wang L, Zhang N. Tumor specific delivery and therapy by double-targeted nanostructured lipid carriers with anti-VEGFR-2 antibody. *Mol Pharm* 2011;**8**:2291−301.
22. Bao QY, Zhang N, Geng DD, Xue JW, Merritt M, Zhang C, et al. The enhanced longevity and liver targetability of paclitaxel by hybrid liposomes encapsulating paclitaxel-conjugated gold nanoparticles. *Int J Pharm* 2014;**477**:408−15.
23. Wang X, Chen Y, Dahmani FZ, Yin L, Zhou J, Yao J. Amphiphilic carboxymethyl chitosan-quercetin conjugate with P-gp inhibitory properties for oral delivery of paclitaxel. *Biomaterials* 2014;**35**:7654−65.
24. Lien S, Pastor R, Sutherlin D, Lowman HB. A substrate-phage approach for investigating caspase specificity. *Protein J* 2004;**23**:413−25.
25. Jiang J, Li L, He X, Yi Q, He B, Cao J, et al. Overcoming drug-resistant lung cancer by paclitaxel loaded dual-functional liposomes with mitochondria targeting and pH-response. *Biomaterials* 2015;**52**:126−39.
26. Mu H, Lin KX, Zhao H, Xing S, Li C, Liu F, et al. Identification of biomarkers for hepatocellular carcinoma by semiquantitative immunocytochemistry. *World J Gastroenterol* 2014;**20**:5826−38.
27. Seymour LW, Ferry DR, Anderson D, Hesslewood S, Julyan PJ, Poyner R, et al. Hepatic drug targeting: phase I evaluation of polymer-bound doxorubicin. *J Clin Oncol* 2002;**20**:1668−76.
28. Gao YY, Chen H, Zhou YY, Wang LT, Hou Y, Xia XH, et al. Intra-organ ttargeting of gold conjugates for precise liver cancer treatment. *ACS Appl Mater Interfaces* 2017;**9**:31458−68.
29. Ding Y, Liang JJ, Geng DD, Wu D, Dong L, Shen WB, et al. Development of a liver-targeting gold-PEG-galactose nanoparticle platform and a structure-function study. *Part Part Syst Char* 2014;**31**:347−56.
30. Hoye AT, Davoren JE, Wipf P, Fink MP, Kagan VE. Targeting mitochondria. *Acc Chem Res* 2008;**41**:87−97.
31. Qu Q, Ma X, Zhao Y. Targeted delivery of doxorubicin to mitochondria using mesoporous silica nanoparticle nanocarriers. *Nanoscale* 2015;**7**:16677−86.
32. Shchepinova MM, Cairns AG, Prime TA, Logan A, James AM, Hall AR, et al. MitoNeoD: a mitochondria-targeted superoxide probe. *Cell Chem Biol* 2017;**24**:1285−98.
33. Zhang N, Chen H, Liu AY, Shen JJ, Shah V, Zhang C, et al. Gold conjugate-based liposomes with hybrid cluster bomb structure for liver cancer therapy. *Biomaterials* 2015;**74**:280−91.
34. Yang X, Hu C, Tong F, Liu R, Zhou Y, Qin Y, et al. Tumor microenvironment-responsive dual drug dimer-loaded pegylated bilirubin nanoparticles for improved drug delivery and enhanced immune-chemotherapy of breast cancer. *Adv Funct Mater* 2019;**29**:1901896.
35. Li J, Wang F, Sun D, Wang R. A review of the ligands and related targeting strategies for active targeting of paclitaxel to tumours. *J Drug Target* 2016;**24**:590−602.
36. Xu Z, Wang S, Li Y, Wang M, Shi P, Huang X. Covalent functionalization of graphene oxide with biocompatible poly(ethylene glycol) for delivery of paclitaxel. *ACS Appl Mater Interfaces* 2014;**6**:17268−76.
37. Yardley DA. nab-Paclitaxel mechanisms of action and delivery. *J Control Release* 2013;**170**:365−72.
38. Thornberry NA, Rano TA, Peterson EP, Rasper DM, Timkey T, Garcia-Calvo M, et al. A combinatorial approach defines specificities of members of the caspase family and granzyme B: functional relationships established for key mediators of apoptosis. *Biol Chem* 1997;**272**:17907−11.
39. Khosravi-Far K, Esposti MD. Death receptor signals to mitochondria. *Cancer Biol Ther* 2004;**3**:1051−7.
40. Hou XS, Wang HS, Mugaka BP, Yang GJ, Ding Y. Mitochondria: promising organelle targets for cancer diagnosis and treatment. *Biomater Sci* 2018;**6**:2786−97.
41. Wang Q, Hu W, Feng Q, Cao XH, Chai W, Yi C, et al. Coumarin-modified gold nanoprobes for the sensitive detection of caspase-3. *RSC Adv* 2015;**5**:43824−30.
42. Zhang X, Li D, Huang J, Ou K, Yan B, Shi F, et al. Screening of pH-responsive long-circulating polysaccharide−drug conjugate nanocarriers for antitumor applications. *J Mater Chem B* 2019;**7**:251−64.